AIAA 2001-2162

Imposition of Oscillatory Waves Inside a Cylindrical Tube with Large Wall Suction

Todd A. Jankowski and Joseph Majdalani
Marquette University
Milwaukee, WI 53233

7th AIAA/CEAS Aeroacoustics Conference
28–30 May 2001
Maastricht, The Netherlands

Imposition of Oscillatory Waves inside a Cylindrical Tube with Large Wall Suction

T. A. Jankowski* and J. Majdalani†
Marquette University, Milwaukee, WI 53233

This study considers the laminar oscillatory flow in a porous tube with uniform wall suction. For a low aspect ratio tube, the time-dependent governing equations are decomposed following a regular perturbation of the dependent variables. The method of matched-asymptotic expansions is then used to obtain a solution for the unsteady momentum equation developing from flow decomposition. The numerically verified end results suggest that the asymptotic scheme is capable of providing a sufficiently accurate solution. This is due to the error associated with the matched-asymptotic expansion being smaller than the error introduced while linearizing the Navier-Stokes equations. A basis for comparison is established by examining the evolution of the oscillatory field in both space and time. The corresponding boundary-layer behavior is also characterized over a range of oscillation frequencies and wall suction velocities. In general, the current solution is found to exhibit features that are consistent with the laminar theory of periodic flows. By comparison to the exact Sexl profile established in nonporous tubes, the current critically-damped solution exhibits a slightly smaller overshoot and depth of penetration. These features may be attributed to the suction effect that tends to attract the shear layers closer the wall.

I. Introduction

THE purpose of this paper is to derive a closed-form analytical solution for the oscillatory velocity field in a porous tube with large wall suction. The governing equations will be solved for the unsteady laminar flow using the assumption of axial symmetry. Flow decomposition will be feasible using standard perturbation techniques. The scope will be limited to cases for which the cross-flow Reynolds number based on the wall suction velocity v_w and tube radius a is large $\left(R = v_w a / \nu \geq 20\right)$.

Suction-induced flows of this type arise in the modeling of the respiratory function in the lungs and airways, in the design of hydraulic line transmissions, in sweat cooling, and in boundary-layer control. Past studies have primarily concentrated on the non-oscillatory flow developed due to mass extraction at the boundaries. This study attempts to account for possible flow periodicity that can be often introduced either internally, through a self-sustaining mechanism, or externally, through an oscillating boundary.

Examples of self-induced oscillatory motions can be realized in many practical flows. The reason is that pressure oscillations that take place at random frequencies can be unavoidable due to small inevitable fluctuations in the wall suction rate. Those pressure waves that are excited at the tube's natural frequency go on to promote a self-sustaining oscillatory field. Conversely, there are numerous flow models applicable to permeable tubes that exhibit an externally-induced oscillatory motion. One may cite the modeling of the respiratory and circulatory functions in biological organisms. Irrespective of the source of periodicity, this study will attempt to derive the solution for the oscillatory field in the presence of large wall suction and laminar conditions.

Berman's landmark paper[1] precipitated a number of interesting investigations into the laminar porous flow problem. Incidentally, Berman was the first to use asymptotics in solving for the mean component developed in flows with very small suction. This was

*Graduate Student and Research Associate. Member AIAA.
†Assistant Professor, Department of Mechanical and Industrial Engineering. Member AIAA.

accomplished after reducing the Navier-Stokes equations into a single, non-linear ordinary differential equation (ODE) of fourth order. Based on Berman's equation, numerous studies ensued, some with the purpose of generating descriptions for suction-driven flows over different ranges of R. In fact, Yuan,[2,3] Sellars,[4] and Terrill[5,6] have extended Berman's small suction case to encompass higher ranges of R. While Yuan extended Berman's solution to $R = 20$ in both channels and tubes, Sellars and Terrill developed approximate solutions that became exact as $R \to \infty$.

In addition to these studies, other investigations have addressed the issues of flow stability and multiplicity.[7-16] For the cylindrical tube, a total of four solutions, some of which being unstable, have been detected over large ranges of R.[17] In summary, it was found that two solutions existed in the range $0 \le R \le 2.3$, no solutions existed for $2.3 < R < 9.1$, while four possible solutions appeared for $9.1 \le R < \infty$. It should be noted that the leading-order solution for large R that will be used throughout this work was proven to be temporally stable.[17] Since our approach relies on time-dependent perturbations to arrive at a closed-form solution, the scope of this article will be limited to stable solutions only.

The mathematical modeling starts in Sec. II with a definition of the basic flow model. This is initiated with a description of the system geometry and physical criteria. In Sec. III, the governing equations are presented in their general dimensional form. Subsequently, equations and variables are normalized, linearized and decomposed into steady and time-dependent sets. The temporal field is further decomposed using the momentum transport formulation in Sec. IV. This decomposition produces acoustic and vortical equations. The first, pressure-driven response is dealt with immediately, while the second, vorticity-driven component is split using separation of variables. At the outset, it can be realized that a successful assault on the problem is contingent upon solving the separated equation in the radial direction. The latter turns out to be a second order ODE involving two perturbation parameters. To proceed, the distinguished limit and boundary-layer form are determined from a systematic scaling analysis in Sec. V. This is followed in Sec. VI by the presentation of a composite solution based on matched-asymptotic expansions. Finally, in Sec. VII results are displayed and discussed.

II. The Basic Flow Model

A. The Porous Tube

A long slender tube is considered here with porous walls at a radius a. Fluid is extracted from the porous surface at a uniform wall velocity v_w. The length of the tube is defined by L and the system can be simplified by imposing the condition of symmetry about the tube's axis. An axisymmetric flow can thus be realized when variations in the θ-direction are ignored. This enables the solution domain to become reducible to $0 \le x \le l$, and $0 \le r \le 1$, where $l = L/a$ is the dimensionless tube length. For illustrative purposes, Fig. 1 is used to present a cross-section of the tube with the meanflow streamlines calculated from Terrill's solution for large suction.[6]

Under the influence of small variations in the suction rate, a tube that is closed at the head end and open at the aft end can develop longitudinal pressure oscillations of amplitude A. The corresponding acoustic frequency can be specified by[18,19]

$$\omega_s = (m - ½)\pi a_s / L, \tag{1}$$

where a_s is the speed of sound, and m is the oscillation mode number.

B. Limiting Conditions

In order to simplify the analysis to the point where an analytical solution can be arrived at, several restrictions must be observed. First, the meanflow must be Newtonian, laminar, and unsusceptible to mixing, swirling, or turbulence. Furthermore, the oscillatory pressure amplitude is taken to be small in comparison with the stagnation pressure.

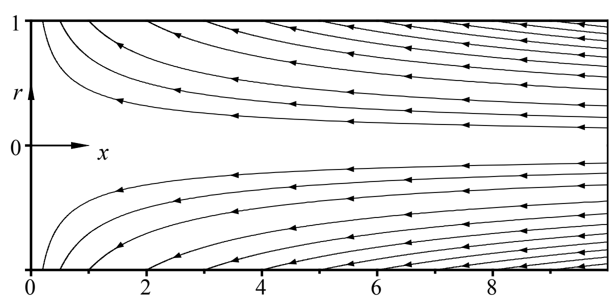

Fig. 1 System geometry showing meanflow streamlines based on Terrill's large suction-flow solution.

III. Governing Equations

A. The Conservation Equations

Employing asterisks to designate dimensional variables, density, pressure, time, velocity, and the shear stress tensor can be represented by ρ^*, p^*, t^*, $\boldsymbol{u}^*$, and τ^*, respectively. Continuity and conservation of momentum can then be written in their general forms[20]

$$\partial\rho^*/\partial t^* + \nabla^*\cdot(\rho^*\boldsymbol{u}^*) = 0 \qquad (2)$$

$$\partial(\rho^*\boldsymbol{u}^*)/\partial t^* + \nabla^*\cdot(\rho^*\boldsymbol{u}^*\boldsymbol{u}^*) = -\nabla^* p^* - (\nabla^*\cdot\tau^*)\,. \qquad (3)$$

By using continuity to simplify Eq. (3) and viscous transfer for a Newtonian fluid, one can transform Eq. (3) into

$$\rho^*\left[\partial\boldsymbol{u}^*/\partial t^* + (\boldsymbol{u}^*\cdot\nabla^*)\boldsymbol{u}^*\right] = -\nabla^* p^* + \mu^*\left[4\nabla^*(\nabla^*\cdot\boldsymbol{u}^*)/3 - \nabla^*\times(\nabla^*\times\boldsymbol{u}^*)\right] \qquad (4)$$

where μ^* is the dynamic viscosity.

To be general, dimensionless parameters are introduced. Spatial coordinates are hence normalized by a, while velocity and time are made dimensionless by a_s and ω_s, respectively. In summary, we let

$$x = x^*/a\,,\ r = r^*/a\,,\ t = \omega_s t^*,\ \boldsymbol{u} = \boldsymbol{u}^*/a_s\,,\ p = p^*/(\gamma p_s) \text{ and } \rho = \rho^*/\rho_s\,, \qquad (5)$$

where γ is the ratio of specific heats, and ρ_s and p_s are the stagnation density and pressure. Following this choice, Eqs. (2) and (4) become

$$\omega\partial\rho/\partial t + \nabla\cdot(\rho\boldsymbol{u}) = 0\,, \qquad (6)$$

$$\rho[\omega\partial\boldsymbol{u}/\partial t + (\boldsymbol{u}\cdot\nabla)\boldsymbol{u}] = -\nabla p + M\varepsilon\left[4\nabla(\nabla\cdot\boldsymbol{u})/3 - \nabla\times(\nabla\times\boldsymbol{u})\right]. \qquad (7)$$

Equations (6)–(7) follow the definitions of the non-dimensional frequency $\omega \equiv \omega_s a/a_s$, the suction Mach number $M \equiv v_w/a_s$, and the small parameter $\varepsilon \equiv 1/R$.

B. Perturbed Variables

With the introduction of small amplitude oscillations at a frequency ω_s, the instantaneous pressure can be expressed as the linear sum of time-dependent and steady components:

$$p = p_0 + \bar{\varepsilon} p_1 \exp(-it)\,, \qquad (8)$$

where $i = \sqrt{-1}$, $\bar{\varepsilon} = A/(\gamma p_s)$, and (p_0, p_1) are spatial functions. Noting that the meanflow solution is incompressible, small compressibility effects can only influence the time-dependent field. Density can thus be normalized by its mean component and expanded in a similar fashion viz.

$$\rho = 1 + \bar{\varepsilon}\rho_1 \exp(-it)\,. \qquad (9)$$

The total velocity can also be expanded as

$$\boldsymbol{u} = M\boldsymbol{u}_0 + \bar{\varepsilon}\boldsymbol{u}_1 \exp(-it)\,. \qquad (10)$$

The Mach number multiplies $\boldsymbol{u}_0$ because the latter is the meanflow velocity normalized by v_w.

C. Leading-order Decomposition

Equations (8)–(10) can be inserted back into Eqs. (6)–(7). The zero-order terms yield the meanflow equations

$$\nabla\cdot\boldsymbol{u}_0 = 0 \qquad (11)$$

$$M^2(\boldsymbol{u}_0\cdot\nabla)\boldsymbol{u}_0 = -\nabla p_0 + M^2\varepsilon\left[4\nabla(\nabla\cdot\boldsymbol{u}_0)/3 - \nabla\times(\nabla\times\boldsymbol{u}_0)\right]. \qquad (12)$$

Following Berman,[1] a steady streamfunction can be defined by

$$\Psi = -xF(r)\,. \qquad (13)$$

Subsequently, the velocity can be expressed by $(u_0, v_0) = [-xF'(r)/r, F(r)/r]$. By substituting these definitions into Eq. (12), Terrill has shown that $F = r^2$ will correspond to the exact meanflow solution for the infinitely large suction case.[6] The mean pressure arising in this context can be integrated from Eq. (12) to obtain

$$p_0(x,r) = 1/\gamma - M^2 r^2(1+x^2)/2\,. \qquad (14)$$

D. Time-dependent Equations

Terms of $\mathcal{O}(\bar{\varepsilon})$ in Eqs. (6)-(7) lead to

$$-i\omega\rho_1 + \nabla\cdot\boldsymbol{u}_1 = -M\nabla\cdot(\rho_1\boldsymbol{u}_0)\,, \qquad (15)$$

$$-i\omega\boldsymbol{u}_1 = -M\left[\nabla(\boldsymbol{u}_0\cdot\boldsymbol{u}_1) - \boldsymbol{u}_1\times(\nabla\times\boldsymbol{u}_0) - \boldsymbol{u}_0\times(\nabla\times\boldsymbol{u}_1)\right] - \nabla p_1 + M\varepsilon\left[4\nabla(\nabla\cdot\boldsymbol{u}_1)/3 - \nabla\times(\nabla\times\boldsymbol{u}_1)\right]. \qquad (16)$$

Equations (15) and (16) describe the intimate coupling between mean and unsteady motions. They clearly indicate that the wall suction velocity $\boldsymbol{u}_0$ can strongly influence the oscillatory flow motion.

IV. Momentum Transport Formulation

A. Irrotational and Solenoidal Vectors

In order to proceed, temporal disturbances can be split into solenoidal and irrotational components. Using a circumflex to denote the curl-free pressure-driven part, and a tilde for the divergence-free boundary-driven part, the time-dependent velocity component can be expressed as

$$\boldsymbol{u}_1 = \hat{\boldsymbol{u}} + \tilde{\boldsymbol{u}} \tag{17}$$

with $$\nabla \times \boldsymbol{u}_1 = \nabla \times \tilde{\boldsymbol{u}}\,,\ p_1 = \hat{p}\,,\ \rho_1 = \hat{\rho}\,. \tag{18}$$

This decomposition charges all vortices to the solenoidal field, and compressibility sources and sinks to the irrotational field.

B. The Linearized Navier-Stokes Equations

Insertion of Eqs. (17)-(18) into Eqs. (15)-(16) leads to two independent sets that are coupled through the boundary conditions at the wall. These responses are byproducts of pressure-driven and vorticity-driven oscillation modes at $\mathcal{O}(\bar{\varepsilon})$. While the acoustic, compressible, and irrotational equations collapse into

$$-i\omega\hat{\rho} + \nabla\cdot\hat{\boldsymbol{u}} = -M\nabla\cdot\left(\hat{\rho}\boldsymbol{u}_0\right), \tag{19}$$

$$-i\omega\hat{\boldsymbol{u}} = -\nabla\hat{p} + 4M\varepsilon\nabla\left(\nabla\cdot\hat{\boldsymbol{u}}\right)/3$$
$$-M\left[\nabla\left(\hat{\boldsymbol{u}}\cdot\boldsymbol{u}_0\right) - \hat{\boldsymbol{u}}\times\left(\nabla\times\boldsymbol{u}_0\right)\right], \tag{20}$$

the rotational and incompressible set is comprised of

$$\nabla\cdot\tilde{\boldsymbol{u}} = 0\,, \tag{21}$$

$$-i\omega\tilde{\boldsymbol{u}} = -M\varepsilon\nabla\times\left(\nabla\times\tilde{\boldsymbol{u}}\right)$$
$$-M\left[\nabla\left(\tilde{\boldsymbol{u}}\cdot\boldsymbol{u}_0\right) - \tilde{\boldsymbol{u}}\times\left(\nabla\times\boldsymbol{u}_0\right) - \boldsymbol{u}_0\times\left(\nabla\times\tilde{\boldsymbol{u}}\right)\right]. \tag{22}$$

C. Coupling Conditions

Two boundary conditions must be satisfied by the unsteady velocity component $\boldsymbol{u}_1$. These are the no-slip condition at the wall $u_1(x,1) = 0$, and symmetry about the midsection plane, $\partial u_1(x,0)/\partial r = 0$.

D. Pressure-driven Solution

When Eq. (19) is multiplied by $-i\omega$, the divergence of Eq. (20) can be evaluated; resulting terms can be added to produce the following wave equation:

$$\nabla^2\hat{p} + \omega^2\hat{p} = -4M\varepsilon\nabla^2\left(\nabla\cdot\hat{\boldsymbol{u}}\right)/3$$
$$-M\left\{i\omega\nabla\cdot\left(\boldsymbol{u}_0\hat{p}\right) - \nabla^2\left(\hat{\boldsymbol{u}}\cdot\boldsymbol{u}_0\right)\right.$$
$$\left.+\nabla\cdot\left[\hat{\boldsymbol{u}}\times\left(\nabla\times\boldsymbol{u}_0\right)\right]\right\}. \tag{23}$$

A solution at $\mathcal{O}(M)$ can be readily achieved through separation of variables and closed-open boundary conditions. The ensuing acoustic pressure and velocity are

$$\hat{p} = \cos(\omega x) + \mathcal{O}(M)\,, \tag{24}$$

$$\hat{\boldsymbol{u}} = i\sin(\omega x)\,\hat{e}_x + \mathcal{O}(M)\,. \tag{25}$$

E. Vortical Equations

Assuming that the ratio of the normal to axial velocity is of the same order as the Mach number (i.e. $\tilde{v}/\tilde{u} = \mathcal{O}(M)$, $\tilde{v}$ can be dropped at leading order. This assumption can be justified in view of the arguments presented by Flandro[21] and Majdalani and Van Moorhem.[22] Applying this condition, along with the definition of the meanflow velocity, the axial momentum equation reduces to

$$iS\tilde{u} = \frac{\partial\left(\tilde{u}u_0\right)}{\partial x} + v_0\frac{\partial\tilde{u}}{\partial r} - \frac{\varepsilon}{r}\frac{\partial}{\partial r}\left(r\frac{\partial\tilde{u}}{\partial r}\right) + \mathcal{O}(M) \tag{26}$$

where $S \equiv \omega/M$ is the Strouhal number. When expressed in terms of the meanflow streamfunction, Eq. (26) becomes

$$\left(iS + \frac{F'}{r}\right)\tilde{u} = \frac{F}{r}\frac{\partial\tilde{u}}{\partial r} - \frac{xF'}{r}\frac{\partial\tilde{u}}{\partial x}$$
$$-\frac{\varepsilon}{r}\frac{\partial}{\partial r}\left(r\frac{\partial\tilde{u}}{\partial r}\right) + \mathcal{O}(M)\,. \tag{27}$$

A solution for Eq. (27) will be presented next.

F. The Separable Boundary-layer Equation

A solution for Eq. (27) can be developed through the use of separation of variables. Assuming the form

$$\tilde{u}(x,r) = X(x)Y(r)\,, \tag{28}$$

substitution into Eq. (27) leads to

$$\frac{x}{X}\frac{\mathrm{d}X}{\mathrm{d}x} = \frac{F}{F'Y}\frac{\mathrm{d}Y}{\mathrm{d}r} - \frac{\varepsilon r}{F'Y}\frac{\mathrm{d}^2Y}{\mathrm{d}r^2}$$
$$-\frac{\varepsilon}{F'Y}\frac{\mathrm{d}Y}{\mathrm{d}r} - \frac{iSr}{F'} - 1 = \kappa_n \tag{29}$$

where $\kappa_n > 0$ is the separation eigenvalue. Integration of the x-equation can be performed easily and then inserted into Eq. (28). The outcome is

$$\tilde{u}(x,r) = \sum_n c_n x^{\kappa_n} Y_n(r)\,, \tag{30}$$

where c_n is the integration constant for each κ_n. Satisfaction of the no-slip condition at the wall requires setting the acoustic and vortical velocity components equal and opposite at $r=1$. One finds

$$\tilde{u}(x,1) = -i\sin(\omega x)\,. \tag{31}$$

Using a series expansion of the sine function, and setting the result equal to Eq. (30), one gets

$$\sum_n c_n x^{\kappa_n} Y_n(1) = -i\sum_{n=0}^{\infty}\frac{(-1)^n(\omega x)^{2n+1}}{(2n+1)!}\,. \tag{32}$$

Equating terms necessitates that

$$\kappa_n = 2n+1,\ c_n = -i\frac{(-1)^n\omega^{2n+1}}{(2n+1)!},\ Y_n(1)=1\,, \tag{33}$$

where $n = 0,1,2,\ldots\infty$. The rotational velocity component becomes

$$\tilde{u}(x,r) = -i\sum_{n=0}^{\infty}\frac{(-1)^n(\omega x)^{2n+1}}{(2n+1)!}Y_n(r)\,. \tag{34}$$

In order to bring closure to Eq. (34), Y_n needs to be determined from Eq. (29). One finds that Y_n must be obtained from the doubly-perturbed boundary-value problem

$$\varepsilon\frac{\mathrm{d}^2Y_n}{\mathrm{d}r^2} + \left(-\frac{F}{r}+\frac{\varepsilon}{r}\right)\frac{\mathrm{d}Y_n}{\mathrm{d}r} + \left[iS + (2n+2)\frac{F'}{r}\right]Y_n = 0 \tag{35}$$

where

$$Y_n(1) = 1\,,\ Y_n{}'(0) = 0\,. \tag{36}$$

These two boundary conditions stem from the no slip and core symmetry requirements.

V. Boundary-layer Analysis

Substitution of Terrill's meanflow solution into Eq. (35) leads to

$$\varepsilon\frac{\mathrm{d}^2Y_n}{\mathrm{d}r^2} + (-r+\varepsilon/r)\frac{\mathrm{d}Y_n}{\mathrm{d}r} + [iS + (4n+4)]Y_n = 0\,. \tag{37}$$

In what follows, Eq. (37) will be solved using the method of matched-asymptotic expansions. To that end, the perturbation parameters need to be first identified. Since our concern is with solutions corresponding to large R, the primary perturbation parameter is clearly $\varepsilon = R^{-1} \ll 1$. Furthermore, one must recognize that the condition of $S \gg 1$ is necessary to ensure a sufficiently oscillatory flow. Otherwise, the flow becomes quasi-steady.

Asymptotic approximations to Eq. (37) depend on the development of a relationship between the two perturbation parameters present in the problem. By inspection of numerical simulations carried out for the large suction case, one comes to the conclusion that the problem exhibits a typical second-order wave type response that bears a strong resemblance to a critically-damped wave. On that account, a distinguished limit will be needed to relate ε and S in a manner to produce the expected response.

To start, an order of magnitude relationship between the control parameters must be posited. For example, one can let

$$S \sim \mathcal{O}\left(\varepsilon^{-\zeta}\right). \tag{38}$$

Also, rescaling of the viscous domain requires a distortion of the independent variable in the form

$$1 - r = \varepsilon^k z\,. \tag{39}$$

In order to determine the distinguished limit, one may apply the stretching transformation and use $S = \varepsilon^{-\zeta}$ in Eq. (37). The result is

$$\varepsilon^{1-2k}\frac{\mathrm{d}^2Y_n}{\mathrm{d}z^2} + \varepsilon^{-k}(r-\varepsilon/r)\frac{\mathrm{d}Y_n}{\mathrm{d}z} + \left[i\varepsilon^{-\zeta} + (4n+4)\right]Y_n = 0\,. \tag{40}$$

For a critically damped response to occur near the wall, a balance between all three terms in Eq. (40) must be established. Clearly, all terms will be in balance when $\zeta = k = 1$. These distinctive orders indicate that the boundary-layer thickness is of $\mathcal{O}(\varepsilon)$ and that,

$$S = \mathcal{O}\left(\varepsilon^{-1}\right). \tag{41}$$

It may be interesting to note that these distinguished limits are dissimilar from those arising in the injection flow analogue.[23] The disparity can be attributed to the reversal in the physics of the problem, namely, in the relocation of the viscous boundary layer to the vicinity of the wall when suction is imposed.

VI. Matched-asymptotic Expansions

A. The Relevant Scales

In order to proceed, the characteristic length scale necessary to magnify the thin viscous region near the wall needs to be identified. From the foregoing order of magnitude analysis, the relevant scales can be recognized to be $r = r$ in the outer domain, and

$$z = (1-r)/\varepsilon \tag{42}$$

in the inner region. Solving the problem with matched-asymptotic expansions involves the formulation of two separate solutions over the domain of interest. While Eq. (37) is only valid in the outer domain (i.e., the inviscid region), a transformed equation is needed to capture the rapid variations near the wall (inside the viscous boundary layer). In both cases, we find it convenient to multiply Eq. (37) by r and write the governing equation as

$$\varepsilon r\frac{\mathrm{d}^2Y_n}{\mathrm{d}r^2}+\left(-r^2+\varepsilon\right)\frac{\mathrm{d}Y_n}{\mathrm{d}r}+r\left[iS+(4n+4)\right]Y_n=0\,. \quad (43)$$

B. The Outer Solution

Using regular perturbations to construct the outer solution Y_n^o, one may start by expanding

$$Y_n^o=Y_0^o+\varepsilon Y_1^o+\mathcal{O}\left(\varepsilon^2\right). \quad (44)$$

Inserting Eq. (44) into Eq. (43) gives

$$\varepsilon r\frac{\mathrm{d}^2Y_0^o}{\mathrm{d}r^2}-r^2\frac{\mathrm{d}Y_0^o}{\mathrm{d}r}-r^2\varepsilon\frac{\mathrm{d}Y_1^o}{\mathrm{d}r}+\varepsilon\frac{\mathrm{d}Y_0^o}{\mathrm{d}r}+r\left[(4n+4)+iS\right]\left(Y_0^o+\varepsilon Y_1^o\right)+\mathcal{O}\left(\varepsilon^2\right)=0\,. \quad (45)$$

Keeping in mind that $S=\mathcal{O}\left(\varepsilon^{-1}\right)$, the equations defining the first two terms in the outer solution become

$$iSrY_0^o=0 \quad (46)$$

$$iSr\varepsilon Y_1^o=r^2\frac{\mathrm{d}Y_0^o}{\mathrm{d}r}-r\,(4n+4)\,Y_0^o\,. \quad (47)$$

Solving these equations leads to

$$Y_0^o=Y_1^o=0\,,\quad Y_n^o=0+\mathcal{O}(\varepsilon^2)\,. \quad (48)$$

C. The Inner Solution

Having realized that the outer solution is zero, the stretching transformation must now be applied to the original coordinate in order to obtain the inner equation. This procedure converts Eq. (43) into

$$(1-\varepsilon z)\frac{\mathrm{d}^2Y_n^i}{\mathrm{d}z^2}+\left[1-\varepsilon\,(2z+1)+\varepsilon^2z\right]\frac{\mathrm{d}Y_n^i}{\mathrm{d}z}+\left(\varepsilon-\varepsilon^2z\right)\left[(4n+4)+iS\right]Y_n^i=0\,. \quad (49)$$

The inner solution can be similarly expanded using $Y_n^i=Y_0^i+\varepsilon Y_1^i+\mathcal{O}\left(\varepsilon^2\right)$. The result of substitution is

$$(1-\varepsilon z)\frac{\mathrm{d}^2Y_0^i}{\mathrm{d}z^2}+\left(\varepsilon-\varepsilon^2z\right)\frac{\mathrm{d}^2Y_1^i}{\mathrm{d}z^2}+\left[1-\varepsilon\,(2z+1)+\varepsilon^2z\right]\left(\frac{\mathrm{d}Y_0^i}{\mathrm{d}z}+\varepsilon\frac{\mathrm{d}Y_1^i}{\mathrm{d}z}\right)+\left(\varepsilon-\varepsilon^2z\right)\left[(4n+4)+iS\right]\left(Y_0^i+\varepsilon Y_1^i\right)=0\,. \quad (50)$$

Since the inner equation is of second order, two conditions must be imposed on the inner solution at each perturbation level. While the first can be determined from the no-slip at the wall, the second must be concluded via matching with the outer domain. Using Eq. (36) and the expansion for Y_n^i, the boundary condition at the wall gives

$$Y_0^i\,(z=0)=1\,,\quad Y_1^i(z=0)=0\,. \quad (51)$$

At this juncture, the leading and first order correction terms can be readily found. From Eq. (50), the $\mathcal{O}(1)$ equation reads

$$\frac{\mathrm{d}^2Y_0^i}{\mathrm{d}z^2}+\frac{\mathrm{d}Y_0^i}{\mathrm{d}z}+iS\varepsilon Y_0^i=0\,, \quad (52)$$

wherefore

$$Y_0^i=c_1\exp\left[\tfrac{1}{2}\left(\sqrt{1-4iS\varepsilon}-1\right)z\right]+c_2\exp\left[-\tfrac{1}{2}\left(\sqrt{1-4iS\varepsilon}+1\right)z\right]. \quad (53)$$

Straightforward application of the boundary condition at the wall renders

$$c_2=1-c_1\,. \quad (54)$$

Hence,

$$Y_0^i=c_1\exp\left[\tfrac{1}{2}\left(\sqrt{1-4iS\varepsilon}-1\right)z\right]+\left(1-c_1\right)\exp\left[-\tfrac{1}{2}\left(\sqrt{1-4iS\varepsilon}+1\right)z\right]. \quad (55)$$

Next, the $\mathcal{O}(\varepsilon)$ equation that can be collected from Eq. (50) is

$$\frac{\mathrm{d}^2Y_1^i}{\mathrm{d}z^2}+\frac{\mathrm{d}Y_1^i}{\mathrm{d}z}+iS\varepsilon Y_1^i=z\frac{\mathrm{d}^2Y_0^i}{\mathrm{d}z^2}+(2z+1)\frac{\mathrm{d}Y_0^i}{\mathrm{d}z}-(4n+4-iS\varepsilon z)\,Y_0^i\,. \quad (56)$$

While the homogeneous solution can be evaluated by inspection via

$$Y_{1,\mathrm{h}}^i=B_1\exp\left[\tfrac{1}{2}\left(\sqrt{1-4iS\varepsilon}-1\right)z\right]+B_2\exp\left[-\tfrac{1}{2}\left(\sqrt{1-4iS\varepsilon}+1\right)z\right], \quad (57)$$

the right hand side of Eq. (56) can be rearranged into

$$c_1\left[\tfrac{1}{4}\left(\sqrt{1-4iS\varepsilon}-1\right)^2z+\tfrac{2z+1}{2}\left(\sqrt{1-4iS\varepsilon}-1\right)-(4n+4-iS\varepsilon z)\right]\exp\left[\tfrac{1}{2}\left(\sqrt{1-4iS\varepsilon}-1\right)z\right]$$
$$\left(1-c_1\right)\left[\tfrac{1}{4}\left(\sqrt{1-4iS\varepsilon}+1\right)^2z-\tfrac{2z+1}{2}\left(\sqrt{1-4iS\varepsilon}+1\right)-(4n+4-iS\varepsilon z)\right]\exp\left[-\tfrac{1}{2}\left(\sqrt{1-4iS\varepsilon}+1\right)z\right]. \quad (58)$$

A particular solution must therefore be assumed such that

$$Y_{1,\mathrm{p}}^i=\left(B_3z+B_4z^2\right)\exp\left[\tfrac{1}{2}\left(\sqrt{1-4iS\varepsilon}-1\right)z\right]+\left(B_5z+B_6z^2\right)\exp\left[-\tfrac{1}{2}\left(\sqrt{1-4iS\varepsilon}+1\right)z\right]. \quad (59)$$

After differentiating and substituting Eq. (59) into the left hand side of Eq. (56), equating terms of order 1 and z^2 requires that

$$B_3 = c_1\left[\frac{1}{2} - \frac{\left(4n+\frac{9}{2}\right)}{\sqrt{1-4iS\varepsilon}}\right],\ B_4 = 0\,,$$

$$B_5 = \left(1-c_1\right)\left[\frac{1}{2} + \frac{\left(4n+\frac{9}{2}\right)}{\sqrt{1-4iS\varepsilon}}\right],\ B_6 = 0\,. \tag{60}$$

By writing $Y_1^i = Y_{1,\mathrm{h}}^i + Y_{1,\mathrm{p}}^i$ and enforcing Eq. (51), the inner solution turns into

$$\begin{aligned} Y_n^i = &\left\{c_1 - B_2\varepsilon + c_1 z\varepsilon\left[\frac{1}{2} - \frac{\left(4n+\frac{9}{2}\right)}{\sqrt{1-4iS\varepsilon}}\right]\right\} \\ &\times\exp\left[\tfrac{1}{2}\left(\sqrt{1-4iS\varepsilon}-1\right)z\right] \\ &+\left\{\left(1-c_1\right) + B_2\varepsilon + \left(1-c_1\right)z\varepsilon\left[\frac{1}{2} + \frac{\left(4n+\frac{9}{2}\right)}{\sqrt{1-4iS\varepsilon}}\right]\right\} \\ &\times\exp\left[-\tfrac{1}{2}\left(\sqrt{1-4iS\varepsilon}+1\right)z\right]. \end{aligned} \tag{61}$$

D. Asymptotic Matching

Inner and outer solutions can be readily matched using Prandtl's matching principle.[24] By requiring the inner solution in the outer domain to match the outer solution in the inner domain, one may set

$$Y_n^i\left(z\to\infty\right) = Y_n^o\left(r\to 0\right) = Y_{n,\mathrm{cp}}\,, \tag{62}$$

where $Y_{n,\mathrm{cp}}$ is the common part in the overlap region shared by both inner and outer solutions. In our problem, both the outer and common parts are zero. The inner solution in the outer domain will also vanish according to Eq. (62) if, and only if, $c_1 = B_2 = 0$. These constants bring closure to the inner solution and enable the construction of a uniformly valid composite solution. Hence, by adding the inner and outer solutions, less $Y_{n,\mathrm{cp}}$, one finally obtains

$$\begin{aligned} Y_n\left(r\right) = &\left\{1 + (1-r)\left[\frac{1}{2} + \frac{\left(4n+\frac{9}{2}\right)}{\sqrt{1-4iS\varepsilon}}\right]\right\} \\ &\times\exp\left[-\left(\sqrt{1-4iS\varepsilon}+1\right)\frac{(1-r)}{2\varepsilon}\right]. \end{aligned} \tag{63}$$

E. The Oscillatory Velocity

Insertion of Eq. (63) into Eq. (34) results in an expression for the rotational velocity component. The addition of the acoustic component, given by Eq. (25), enables us to express the total axial velocity as an infinite sum, namely,

$$\begin{aligned} u_1\left(x,r\right) = i&\left(\sin\left(\omega x\right) - \sum_{n=0}^{\infty}\frac{(-1)^n\left(\omega x\right)^{2n+1}}{(2n+1)!}\right. \\ &\times\left\{1 + (1-r)\left[\frac{1}{2} + \frac{\left(4n+\frac{9}{2}\right)}{\sqrt{1-4iS\varepsilon}}\right]\right\} \\ &\left.\times\exp\left[-\left(\sqrt{1-4iS\varepsilon}+1\right)\frac{(1-r)}{2\varepsilon}\right]\right). \end{aligned} \tag{64}$$

Since $(1-r)$ is small near the wall, one may use $n=0$ in the secondary term arising from the first-order inner correction. The resulting expression can be summed, at leading order, over all eigenvalues, and placed in closed form by recognizing and grouping the implicit sine function expansion. This manipulation produces

$$\begin{aligned} u_1\left(x,r\right) = i\sin\left(\omega x\right)&\left\{1 - \left[1 + \frac{(1-r)}{2}\left(1 + \frac{9}{\sqrt{1-4iS\varepsilon}}\right)\right]\right. \\ &\left.\times\exp\left[-\left(\sqrt{1-4iS\varepsilon}+1\right)\frac{(1-r)}{2\varepsilon}\right]\right\}. \end{aligned} \tag{65}$$

The latter is found to be practically equivalent to Eq. (64).

VII. Discussion

A. Temporal Field Decomposition

The decomposition of the time-dependent governing equations presented in Sec. IV, during the momentum transport formulation, was first introduced by Flandro[25] and further developed by Majdalani and co-workers[18,19,22,23,26-30] For porous tubes with wall injection, the momentum transport formulation has provided accurate predictions that could be substantiated using full computational fluid dynamics models. The asymptotic approximations were also shown to agree favorably with experimental data obtained in cold-flow simulations of solid rocket motors. Although the physical nature of the problem changes when suction is introduced, the assumptions used in reducing the governing equations remain valid, irrespective of the direction of the velocity at the wall. By analogy with the injection-driven problem, one may expect the same level of agreement to exist between the asymptotic formulations given here and either numerical or experimental studies of the model at hand. In the absence of experimental data to compare with, numerical simulations will be resorted to.

B. Numerical Verification

The solution developed using matched-asymptotic expansions has been compared to a numerical solution of Eq. (37) obtained from a code that was originally developed for injection-driven flows by Majdalani and Van Moorhem.[22] The algorithm employs a fixed step fifth order Runge-Kutta method with shooting to handle the boundary conditions. For the suction case, the step size used was 1×10^{-6}. In former studies,[23,29,30] the same code was shown to provide satisfactory agreement with experimental data. Therein, the code was also shown to match very closely computational data obtained independently by Yang[31] and Roh[32] who utilized a fully compressible, finite-volume Navier-Stokes solver.[33]

C. Graphical Confirmation

Figure 2 illustrates the agreement between the numerical solution and Eq. (63). Over typical ranges of physical parameters, the graphical comparison clearly indicates that the matched-asymptotic solution is in close agreement with the numerical. From the graph, the accuracy of the approximate formulation is seen to increase with increasing Reynolds and Strouhal numbers. This observation is reassuring since it indicates that the solution exhibits the proper asymptotic behavior as $\varepsilon = R^{-1} \to 0$ and $S^{-1} \to 0$. It is also satisfying to note the nearly critical damped-wave response. This rapid damping in both depth and amplitude is consistent with the arguments introduced in Sec. V regarding the scaling orders of S and ε used to obtain the correct distinguished limit. This wave behavior is different from the highly under-damped wave solution associated with injection-driven flows. In the latter, numerous peaks of diminishing amplitude appear as the distance from the wall is increased.

In order to assess the truncation error associated with Eq. (63), the maximum absolute error between asymptotics and numerics is shown in Fig. 3 for the first three eigenvalues and a range of S and R. When plotted versus ε, the error is seen to exhibit a clear asymptotic order as $\varepsilon \to 0$. It also decreases in magnitude with successive increases in S. From the graph, it can be seen that the slope of the error curves and, by the same token, the order of the truncation error approach unity for sufficiently small ε. This confirms the order claimed for the approximation. It should also be noted that the slight increase in the error intercept at higher eigenvalues does not affect the total solution. This is due to the rapid convergence of the series in Eq. (64) as n is increased.

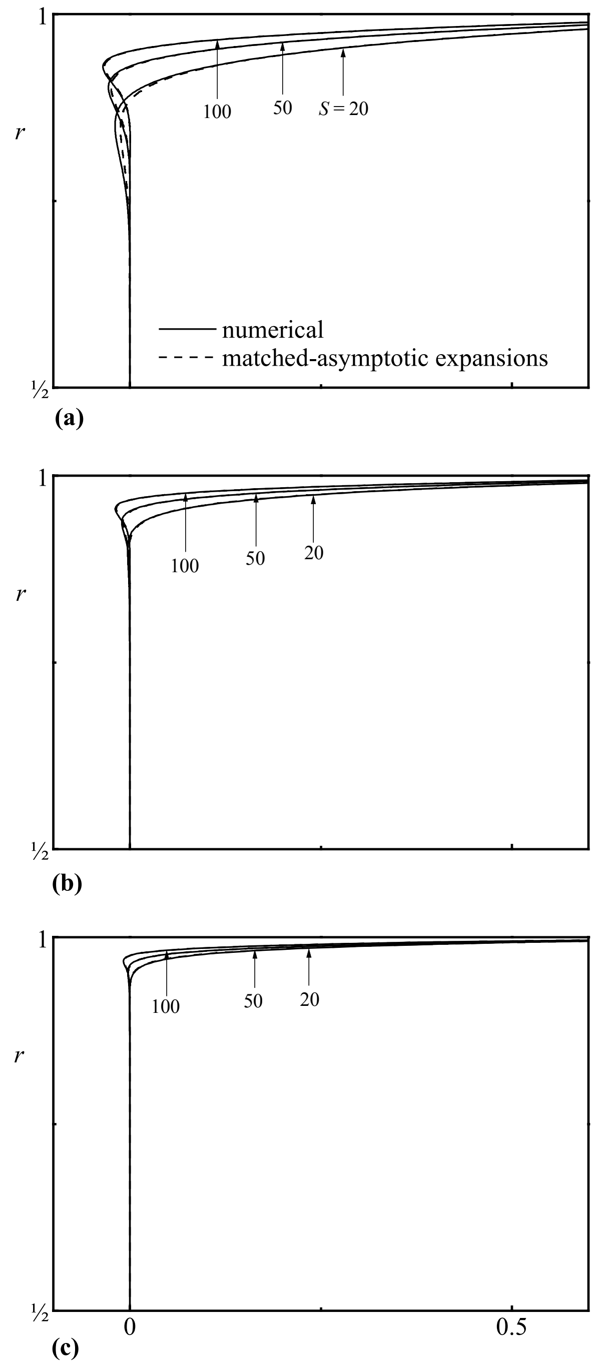

Fig. 2 Here, Y_n is plotted for $n = 0$ over a range of Reynolds and Strouhal numbers. The figures show the slightly under-damped response of the solution for large suction with (a) $R = 20$ and (b) $R = 50$.

D. Variation of Flow Parameters

Figures 4-5 illustrate the effect of varying either the suction velocity or the oscillation frequency on the time-dependent solution. In both figures, the velocity is seen to be a wave traveling in time. While a viscous and rotational layer is present near the wall, a broad inviscid and irrotational region covers the remaining domain. Interestingly, the unsteady velocity reaches a maximum value inside the viscous layer where a small velocity overshoot is realized near the wall. This phenomenon is well known as Richardson's annular effect and seems to be characteristic of oscillatory flows in tubes and channels with and without wall permeation. The small percentage overshoot that accompanies a suction-driven flow is of the same order as that associated with a flow inside a nonporous tube. It is significantly smaller than the 100% overshoot (i.e., velocity doubling) that recurs near the wall of injection-driven flows.

According to the theory of laminar periodic flows, one could expect the magnitude of the velocity overshoot to increase at higher oscillation frequencies. The reason is this. As S is increased, the spatial wavelength diminishes, being inversely proportional to S. The first oscillation peak stemming from a favorable coupling between acoustic and vortical waves will thus occur closer to the wall. Since the rotational component diminishes with the distance from the wall, a larger vortical contribution can be added to the acoustic wave when their coupling occurs closer to the wall (e.g., at higher frequencies). The reduction in spatial wavelength at higher Strouhal numbers increases the rate of viscous dissipation and causes the boundary-layer thickness to decrease.[34] The latter is often referred to as the penetration depth and is a measure of the viscous and rotational layer above the solid boundary.

Figure 4 illustrates the effects of increasing the Reynolds number while decreasing the Strouhal number via an order of magnitude increase in v_w. As the suction speed is increased from Fig. 4a to 4b, the rotational layer is reduced in both depth and overshoot. While the reduction in overshoot can be attributed to

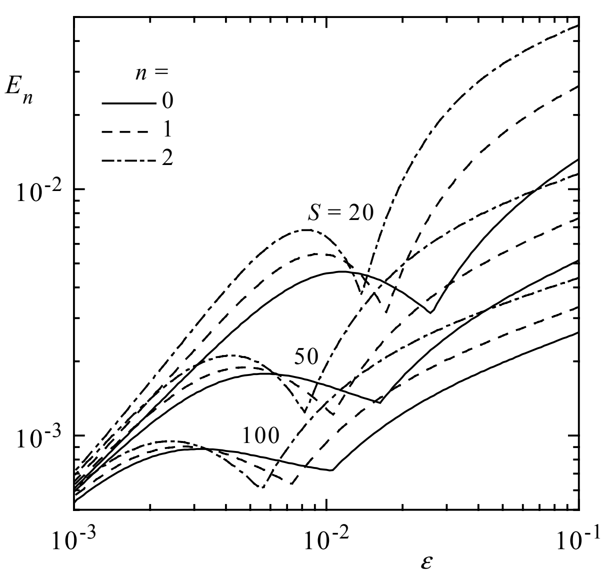

Fig. 3 The maximum error for the approximate solution is plotted vs. ε.

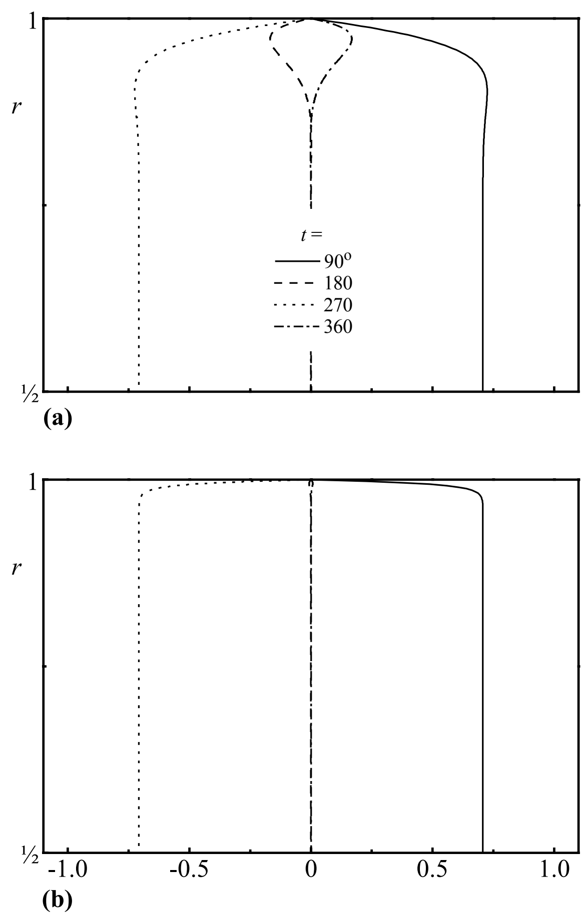

Fig. 4 The oscillatory velocity $u_1 \exp(-it)$ is shown at four different times for $m = 1$ and $x/l = 0.5$. Properties correspond to (a) $R = 20$ and $S = 50$, and (b) $R = 200$ and $S = 5$.

the smaller S and therefore vortical contribution, the smaller depth may be attributed to the increased R. Evidently, the increased fluid withdrawal rate has the effect of attracting the viscous layer closer to the wall.

Figure 5 confirms the previous statements made regarding the oscillation frequency. Clearly, through an order of magnitude increase in S, the penetration depth is decreased, while Richardson's effect is made more appreciable.

E. Oscillation Modes

In closing, Fig. 6 is used to show the spatial evolution of the oscillatory velocity for the first two oscillation modes at $t = 90^\circ$. Also plotted are the amplitudes of the inviscid velocity at sixteen equally spaced times. This is done to illustrate the strong correspondence between the pressure-driven inviscid mode shapes and the spatial distribution of the total velocity. Since the rotational contribution always decays away from the walls, it is clear that the inviscid solution dominates near the core. The spatial amplitude of the oscillatory velocity is thus controlled by the pressure-driven mode shapes associated with the inviscid wave. Except for the small viscous layer that is drawn to the wall by hard suction, the flow is primarily irrotational. In later work, it is hoped that a more general solution could be presented for an oscillatory flow with arbitrary levels of suction.

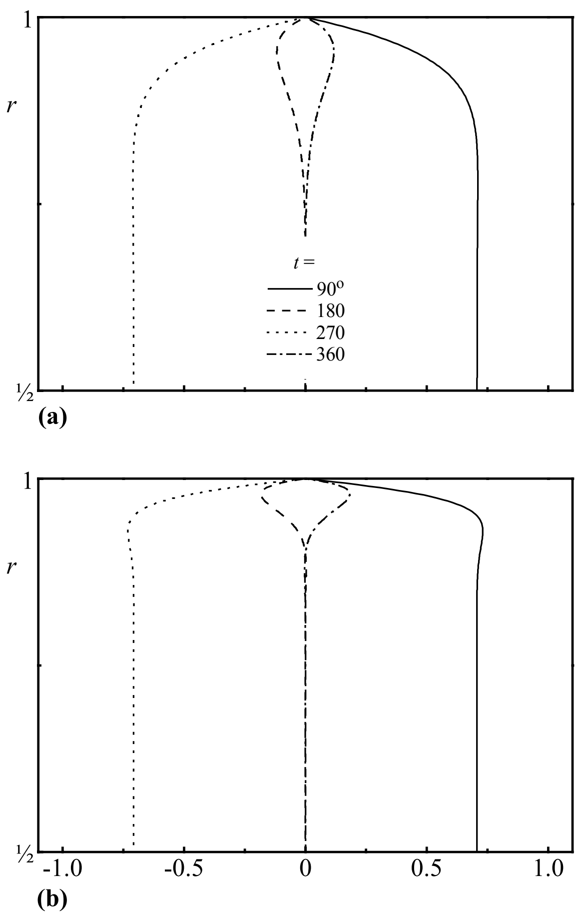

Fig. 5. The velocity $u_1 \exp(-it)$ is plotted for $m = 1$, $x/l = 0.5$, and $R = 20$. Properties correspond (a) $S = 10$, and (b) $S = 100$.

References

[1]Berman, A. S., "Laminar Flow in Channels with Porous Walls," *Journal of Applied Physics,* Vol. 24, No. 9, 1953, pp. 1232-1235.

[2]Yuan, S. W., and Finkelstein, A. B., "Laminar Pipe Flow with Injection and Suction through a Porous Wall," *Transactions of the American Society of Mechanical Engineers: Journal of Applied Mechanics, Series E,* Vol. 78, 1956, pp. 719-724.

[3]Yuan, S. W., "Further Investigation of Laminar Flow in Channels with Porous Walls," *Journal of Applied Physics,* Vol. 27, No. 3, 1956, pp. 267-269.

[4]Sellars, J. R., "Laminar Flow in Channels with Porous Walls at High Suction Reynolds Numbers," *Journal of Applied Physics,* Vol. 26, No. 4, 1955, pp. 489-490.

[5]Terrill, R. M., "Laminar Flow in a Uniformly Porous Channel," *The Aeronautical Quarterly,* Vol. 15, 1964, pp. 299-310.

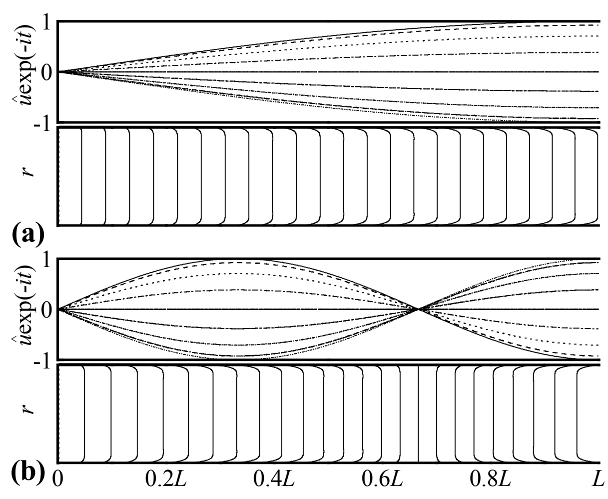

Fig. 6 The first two longitudinal mode shapes for the irrotational velocity are shown at sixteen equally spaced time intervals. In addition, the magnitude of the oscillatory velocity $u_1 \exp(-it)$ is shown for $R = 20$ and $S = 10$. The mode number corresponds to (a) $m = 1$, and (b) $m = 2$. In both plots, the solid curves represent $t = 90^\circ$.

[6]Terrill, R. M., and Thomas, P. W., "On Laminar Flow through a Uniformly Porous Pipe," *Applied Scientific Research, Series A,* Vol. 21, 1969, pp. 37-67.

[7]Robinson, W. A., "The Existence of Multiple Solutions for the Laminar Flow in a Uniformly Porous Channel with Suction at Both Walls," *Journal of Engineering Mathematics,* Vol. 10, No. 1, 1976, pp. 23-40.

[8]Varapaev, V. N., and Yagodkin, V. I., "Flow Stability in a Channel with Porous Walls," *Fluid Dynamics (Izvestiya Akademii Nauk SSSR, Meckanika Zhidkosti i Gaza),* Vol. 4, No. 5, 1969, pp. 91-95.

[9]Zaturska, M. B., Drazin, P. G., and Banks, W. H. H., "On the Flow of a Viscous Fluid Driven Along a Channel by Suction at Porous Walls," *Fluid Dynamics Research,* Vol. 4, No. 3, 1988, pp. 151-178.

[10]Brady, J. F., "Flow Development in a Porous Channel or Tube," *The Physics of Fluids,* Vol. 27, No. 5, 1984, pp. 1061-1067.

[11]Durlofsky, L., and Brady, J. F., "The Spatial Stability of a Class of Similarity Solutions," *The Physics of Fluids,* Vol. 27, No. 5, 1984, pp. 1068-1076.

[12]Hastings, S. P., Lu, C., and MacGillivray, A. D., "A Boundary Value Problem with Multiple Solutions from the Theory of Laminar Flow," *SIAM Journal on Mathematical Analysis,* Vol. 23, No. 1, 1992, pp. 201-208.

[13]Hocking, L. M., "Non-Linear Instability of the Asymptotic Suction Velocity Profile," *Quarterly Journal of Mechanics and Applied Mathematics,* Vol. 28, No. 3, 1975, pp. 341-353.

[14]Lu, C., "On the Asymptotic Solution of Laminar Channel Flow with Large Suction," *SIAM Journal on Mathematical Analysis,* Vol. 28, No. 5, 1997, pp. 1113-1134.

[15]Lu, C., "On the Existence of Multiple Solutions of a Boundary Value Problem Arising from Laminar Flow through a Porous Pipe," *Canadian Applied Mathematics Quarterly,* Vol. 2, No. 3, 1994, pp. 361-393.

[16]Lu, C., MacGillivray, A. D., and Hastings, S. P., "Asymptotic Behaviour of Solutions of a Similarity Equation for Laminar Flows in Channels with Porous Walls," *IMA Journal of Applied Mathematics,* Vol. 49, 1992, pp. 139-162.

[17]Zaturska, M. B., and Banks, W. H. H., "Suction-Driven Flow in a Porous Pipe," *Journal of Applied Mathematics and Mechanics (ZAMM),* Vol. 75, No. 1, 1995, pp. 21-30.

[18]Majdalani, J., "Vorticity Dynamics in Isobarically Closed Porous Channels. Part I: Standard Perturbations," *Journal of Propulsion and Power,* Vol. 17, No. 2, 2001, pp. 355-362.

[19]Majdalani, J., and Roh, T. S., "Vorticity Dynamics in Isobarically Closed Porous Channels. Part II: Space-Reductive Perturbations," *Journal of Propulsion and Power,* Vol. 17, No. 2, 2001, pp. 363-370.

[20]Bird, R. B., Stewart, W. E., and Lightfoot, E. N., *Transport Phenomena*, John Wiley, New York, 1960, p. 78.

[21]Flandro, G. A., "Effects of Vorticity on Rocket Combustion Stability," *Journal of Propulsion and Power,* Vol. 11, No. 4, 1995, pp. 607-625.

[22]Majdalani, J., and Van Moorhem, W. K., "Improved Time-Dependent Flowfield Solution for Solid Rocket Motors," *AIAA Journal,* Vol. 36, No. 2, 1998, pp. 241-248.

[23]Majdalani, J., "The Oscillatory Channel Flow with Arbitrary Wall Injection," *Zeitschrift für angewandte Mathematik und Physik,* Vol. 52, No. 1, 2001, pp. 33-61.

[24]Bender, C. M., and Orszag, S. A., *Advanced Mathematical Methods for Scientists and Engineers*, McGraw-Hill Book Company Inc., New York, 1978.

[25]Flandro, G. A., "Effects of Vorticity Transport on Axial Acoustic Waves in a Solid Propellant Rocket Chamber," in *Combustion Instabilities Driven by Thermo-Chemical Acoustic Sources, Noise Control & Acoustics* American Society of Mechanical Engineers, New York, 1989, Vol. 4, pp. 53-61.

[26]Majdalani, J., "A Hybrid Multiple Scale Procedure for Boundary Layers Involving Several Dissimilar Scales," *Zeitschrift für angewandte Mathematik und Physik,* Vol. 49, No. 6, 1998, pp. 849-868.

[27]Majdalani, J., "Asymptotic Formulation for an Acoustically Driven Field inside a Rectangular Cavity with a Well-Defined Convective Mean Flow Motion," *Journal of Sound and Vibration,* Vol. 223, No. 1, 1999, pp. 73-95.

[28]Majdalani, J., "Vortical and Acoustical Mode Coupling inside a Two-Dimensional Cavity with Transpiring Walls," *Journal of the Acoustical Society of America,* Vol. 106, No. 1, 1999, pp. 46-56.

[29]Majdalani, J., and Roh, T. S., "The Oscillatory Channel Flow with Large Wall Injection," *Proceedings of the Royal Society, Series A,* Vol. 456, No. 1999, 2000, pp. 1625-1657.

[30]Majdalani, J., Flandro, G. A., and Roh, T. S., "Convergence of Two Flowfield Models Predicting a Destabilizing Agent in Rocket Combustion," *Journal of Propulsion and Power,* Vol. 16, No. 3, 2000, pp. 492-497.

[31]Yang, V., and Cai, W., Private communication, Pennsylvania State University, 1998.

[32]Roh, T. S., Private communication, The California Institute of Technology, 1998.

[33]Roh, T. S., Tseng, I. S., and Yang, V., "Effects of Acoustic Oscillations on Flame Dynamics of Homogeneous Propellants in Rocket Motors," *Journal of Propulsion and Power,* Vol. 11, No. 4, 1995, pp. 640-650.

[34]Schlichting, H., *Boundary-Layer Theory*, 7th ed., McGraw-Hill Book Company Inc., New York, 1979.